Emission spectra of alkali-metal (K,Na,Li)−He exciplexes in cold helium gas

K. Enomoto,* K. Hirano, M. Kumakura, Y. Takahashi, and T. Yabuzaki

Department of Physics, Graduate School of Science, Kyoto University, Kyoto 606-8502, Japan
(Received 9 September 2003; published 8 January 2004)

We have observed emission spectra of excimers and exciplexes composed of a light alkali-metal atom in the first excited state and ^{4}He atoms [K*He$_n$ ($n=1-6$), Na*He$_n$ ($n=1-4$), and Li*He$_n$ ($n=1,2$)] in cryogenic He gas (the temperature 2 K$<T<$100 K) in the spectral range from the atomic D lines to 6300 cm^{-1}. Differently from exciplexes with heavier alkali-metal atoms, the spectra for the different number of He atoms were well separated, so that their assignment could be made experimentally. Comparing with the spectra of K*He$_n$, we found that the infrared emission spectrum of the K atom excited in liquid He was from K*He$_6$. To confirm the assignment, we have also carried out *ab initio* calculation of adiabatic potential curves and peak positions of the emission spectra of the exciplexes.

I. INTRODUCTION

Alkali-metal−He excimers and exciplexes M^*He$_n$, where M^* represents an alkali-metal atom in the first excited P state, have very small binding energies (for example, the potential-well depth for the $A\,^2\Pi$ state was calculated by Pascale to be 245 cm^{-1} for K*He, 511 cm^{-1} for Na*He, and 1025 cm^{-1} for Li*He [1]). To investigate this weak interatomic interaction, several spectroscopic studies on M^*He excimers were carried out. Early experiments were made with a thermal alkali-metal vapor in He gas at and above room temperature, so that the emission spectrum of M^*He was observed only as weak and wide red wings of the D emission lines of the alkali-metal atoms [2–5]. Havey and co-workers managed to observe the fluorescence from Na*He and Li*He by using a partially heated cold cell (the temperature $T>100$ K at the fluorescing region) to enhance the excimer formation [6,7]. In addition, the absorption spectrum of the $3d\,^2\Delta\leftarrow2p\,^2\Pi$ bound-bound transition of Li*He was observed above room temperature [8,9]. However, the emission spectra of exciplexes M*He$_n$ ($n\geq2$) have not been observed in thermal vapor cells. To observe the emission spectra of M^*He$_n$ ($n\geq2$) and also to observe clear emission spectra of M^*He, colder He environments are needed.

In this decade, studies on atoms and molecules doped in condensed He have extensively progressed. Dupont-Roc and Kanorsky *et al.* have pointed out that excited alkali-metal atoms in liquid He form exciplexes with He atoms [10,11]. Furthermore, Dupont-Roc discussed that the exciplexes can be classified as whether the fine-structure splitting of an excited alkali-metal atom is larger or smaller than the energy splitting of the excited P state caused by the approach of He atoms [10]. The wave function of the valence electron of the excited alkali-metal atom with the strong spin-orbit coupling holds its applelike shape in liquid He, and hence only two He atoms can approach the alkali-metal atom along the nodal line of the wave function. On the other hand, in the weak

spin-orbit coupling case the wave function is well expressed by the p_z orbital in liquid He, and several He atoms can stick to the alkali-metal atom with forming a ring on the nodal xy plane. So far, it has been found that Cs belongs to the former group [12] and Rb belongs to the latter one [13] from observation of the emission spectrum of the exciplex. Na has also been considered to be an example of the latter group, but the fluorescence from such an exciplex has not yet been observed in liquid He. Following two possible reasons for this can be considered. One is that the fluorescence exists in an unexplored infrared region, and the other is that the fluorescence is quenched due to the level crossing of the electronic excited and ground states [10,11,14]. Similarly to Na, no fluorescence from Li in liquid He has also been observed yet. Differently from Na and Li, we have successfully observed the fluorescence from K*He$_n$ in liquid He, whose spectrum is to be shown later in this paper.

The emission spectrum of the exciplex in liquid He comprises a single spectral component, because exciplex growth is much faster than the radiative decay due to the high density of liquid He. In the following, we will write the terminal exciplex corresponding to this spectral component as M^*He$_{n_{\max}}$. The emission spectra of transient exciplexes M^*He$_n$ ($n<n_{\max}$) are not observed, which makes it difficult to determine the value of $n_{\max}$, especially in the weak spin-orbit coupling case where $n_{\max}>2$. In order to observe the emission spectra of the transient exciplexes, more dilute He environment is needed, so that a He nanodroplet beam and a cold gaseous He environment have been used.

The use of He nanodroplets for investigation of exciplexes was started by the Princeton group. The emission spectra of exciplexes were observed by exciting alkali-metal atoms on the surface of He nanodroplets with a laser beam tuned to the D lines, which also causes detachment of the exciplexes from the surface. They have reported the emission spectra of K*He$_n$ ($n=1,2$) and Na*He$_n$ ($n=1,2$) [15,16], and have revealed the existence of a potential barrier in the detachment of exciplexes from He nanodroplets [17]. The emission spectrum of Rb*He has also been reported by another group [18]. Furthermore, the mass spectroscopy of K*He$_n$ exciplexes detached from the He nanodroplets has been demonstrated [19].

---

*Electronic address: enomoto@yagura.scphys.kyoto-u.ac.jp

The cryogenic gaseous He was used for observation of fluorescence from Ag*He$_n$ ($n = 1,2$) at $T \sim 10$ K [20]. The use of a He gas has advantages that the gas temperature and density can widely be changed. This enables us to control the population distribution among M*He$_n$, so that the observation and the assignment of the emission spectrum for each n can be easily made. Changing the He gas temperature, we could recently observe the emission spectra of all of exciplexes Cs*He$_n$ ($n = 1,2$) and Rb*He$_n$ ($n = 1-6$) in a cold He gas and determine the values of n_{max} for these alkali-metal atoms [12,13].

In the present paper, we report the emission spectra of exciplexes of light alkali-metal atoms, K*He$_n$ ($n = 1-6$), Na*He$_n$ ($n = 1-4$), and Li*He$_n$ ($n = 1,2$), observed in cold gaseous He in the spectral range of the wave number $\nu > 6300$ cm^{-1}. Among these emission spectra, those of K*He$_n$ ($n \geq 3$), Na*He$_n$ ($n \geq 3$), and Li*He$_2$ have not been reported so far. The experimental setup is described in Sec. II. The observed spectra are shown in Sec. III, where we show also the emission spectrum of the K*He$_{n_{max}}$ exciplex in liquid He. In Sec. IV, we confirm the assignments given in Sec. III with the help of *ab initio* calculations.

II. EXPERIMENTAL SETUP

Experimental setup for the observation of emission spectra of exciplexes in cold gaseous He was almost the same as the previous experiments [12,13]. We filled a purified ^{4}He gas (the pressure was about 3.5 atm at room temperature, and the density was 9×10^{19} cm^{-3}) into a Pyrex glass cell, in which a film of Na or K was deposited by distillation. In the case of Li, a piece of metal was placed in the cell, because Li metal could not be transferred into the glass cell by distillation due to corrosiveness of hot Li vapor. After evacuating the glass cell including a piece of Li metal, we heated the cell with a flame up to about the melting point of Li (~ 450 K) for a few seconds to make the surface of the metal clean, and then the He gas was introduced.

The cell was cooled down to the temperature $T < 100$ K in a cryostat chamber. To load an alkali-metal vapor in the cold gaseous He, the second harmonic of a pulsed Nd:YLiF$_4$ (YLF) laser beam (wavelength 523 nm, pulse energy 100 μJ, and repetition rate 1 kHz) was focused on the alkali metal. By this laser ablation method, not only alkali-metal atoms but also clusters were produced. The clusters were reablated by the YLF laser irradiation and were decomposed into atoms. The density of the produced atoms in the YLF laser beam was $\sim 10^9$ cm^{-3}. This laser ablation method was effective for all alkali metals.

The alkali-metal atoms produced in this way were excited through the D_2 transition for K and Na (13 043 cm^{-1} and 16 973 cm^{-1}, respectively) and through the unresolved D transition for Li (14 904 cm^{-1}). We used a cw diode laser for the excitation of K (~ 1 mW/mm^2) and a cw dye laser for the excitation of Na and Li (~ 50 mW/mm^2). The excitation beam was aligned to intersect the ablation laser beam. Spectral profiles of the fluorescence were observed by a spectrometer with a liquid-N$_2$-cooled charge coupled device (CCD) detector, or by a monochromator with an infrared-
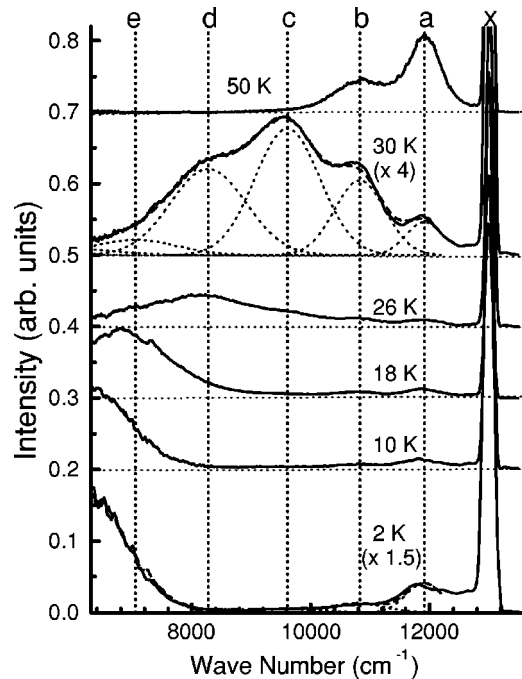

FIG. 1. Emission spectra of K*He$_n$ in the case of D_2 excitation at various temperatures in gaseous He (solid lines). They are normalized by the total intensity integrated over $\nu > 6300$ cm^{-1}. The superposition curves (dashed lines) of five Gaussian curves and the emission spectrum of K*He$_{n_{max}}$ in liquid He (dotted lines) are fitted to the spectra observed at 2 K and 30 K. Vertical dotted lines labeled as $a-e$ indicate the peak positions of the five Gaussian curves for $n = 1-5$, respectively. Sharp emission line labeled as x is the D emission line of atomic K.

sensitive photomultiplier tube (PMT). The CCD system and the PMT system covers the spectral ranges $\nu > 10\,500$ cm^{-1} and $\nu > 6300$ cm^{-1}, respectively. The spectral resolution of the CCD system was about 1.7 nm and that of the PMT system was about 7 nm in the present experiment.

In order to observe an emission spectrum of the exciplex of K in liquid He, we used an unsealed glass cell which was connected to a He gas cylinder placed outside the cryostat chamber. A He gas purified with a liquid-N$_2$-cooled trap was transferred into the cell. The cell was filled with superfluid He at 1.65 K under the saturated vapor pressure. The YLF laser beam ablated a film of K deposited on the cell wall, producing K atoms and clusters into liquid He. The K atoms produced were excited with a cw Ti:Al$_2$O$_3$ laser beam (13 148 cm^{-1}, ~ 200 mW/mm^2). The fluorescence was detected by the PMT system, with which photon counting was started 50 μs after each ablation pulse to avoid the effects of local boiling by ablation.

III. OBSERVED EMISSION SPECTRA

Figure 1 shows the emission spectra of K*He$_n$ observed with the PMT system in gaseous He at various temperatures. We see broadband emission spectra from the exciplexes in addition to the sharp atomic D lines. In the wave number
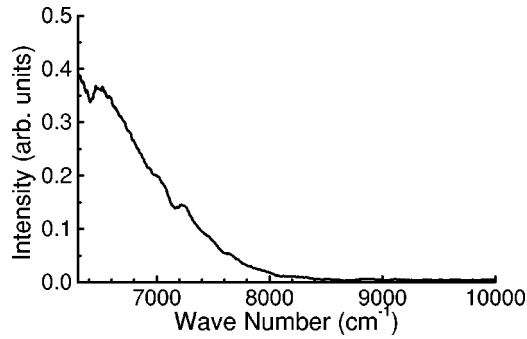
FIG. 2. Emission spectrum of K*He$_{n_{max}}$ in liquid He.

TABLE I. Experimental peak position and width (FWHM) of the spectral component of each exciplex M^*He_n. (a) Peak positions in cm^{-1}. (b) Widths in cm^{-1}.

	(a)		
n	K*He$_n$	Na*He$_n$	Li*He$_n$
1	11 914	14 965	11 553
2	10 826	12 972	~9000
3	9608	10 647	
4	8275	7893	
5	7045		
6	≲6300		

	(b)		
n	K*He$_n$	Na*He$_n$	Li*He$_n$
1	726	1245	1174
2	1005	1741	~2000
3	1295	2523	
4	1498	2551	
5	1621		
6	~1700		

range shown in Fig. 1, the integrated fluorescence intensity from exciplexes relative to the total integrated intensity was about 0.7 at $T<40$ K and it decreased as the temperature was increased from 40 K. At the temperature $T=2$ K, we see an intense spectral component around 6300 cm^{-1}. As the temperature was increased from 10 K, the spectral component was broadened and its peak shifted seemingly toward the larger wave number. However, we see from the spectrum at 30 K that the broadband spectrum was composed of several components. As the temperature was increased up to about 50 K, components at small wave numbers decreased and diminished. These emission spectra are superposition of spectral components from K*He$_n$, and each peak in the undulating structure of the observed spectra corresponds to the spectrum for different n. As seen in the spectrum at 30 K in Fig. 1, there are at least four obvious peaks which are located at about 11 900 cm^{-1}, 10 800 cm^{-1}, 9600 cm^{-1}, and 8300 cm^{-1}. Since the intervals of the peaks are almost the same (~1200 cm^{-1}), they are assigned to the emission from $n=1-4$, respectively. Considering this interval, the red wing around 7000 cm^{-1} of the spectrum at 30 K is assigned mainly to the emission from $n=5$, and the even redder structure appearing at $T<10$ K at about 6300 cm^{-1} is assigned to be from $n=6$. Above assignment will be confirmed in Sec. VI A by our *ab initio* potential calculation.

The emission spectrum of K*He$_{n_{max}}$ observed in liquid He is shown in Fig. 2. The peak is located at a wave number slightly smaller than the detectable limit ($\nu=6300$ cm^{-1}), and the full width at half maximum (FWHM) of this spectrum is roughly estimated to be ~1700 cm^{-1}. No other spectral component was recognized. This emission spectrum agrees well with the redmost spectral component at the temperature $T<10$ K in the gas phase shown in Fig. 1. Therefore, we can conclude that $n_{max}=6$ for K. In the following, the emission spectrum shown in Fig. 2 will be used as that of K*He$_6$.

In order to determine experimentally the peak positions and the widths of spectral components for K*He$_n$ ($n=1-5$), we fitted superposition of five Gaussian curves and the spectrum of K*He$_6$ shown in Fig. 2 to all of the observed spectra shown in Fig. 1. The fitting parameters were the intensities of all the six components at each temperature and the center positions and widths of five Gaussian curves. We assumed here that the peak positions and the widths of all spectral components are independent of the temperature. As

examples, we show the best-fitted superpositions by dashed lines and the six components by dotted lines in Fig. 1, where we see good agreement with the observed spectra at 2 K and 30 K. The obtained peak positions and widths (FWHM) are listed in Table I, together with the results for Na*He$_n$ and Li*He$_n$.

Figure 3 shows the temperature dependence of the population distribution of K*He$_n$ ($n=0-6$), where $n=0$ indicates the K atom in the $4\,{}^2P$ state. The relative population N_n of K*He$_n$ was obtained from $I=\int g_n(\nu)\nu^{-3}d\nu$, where
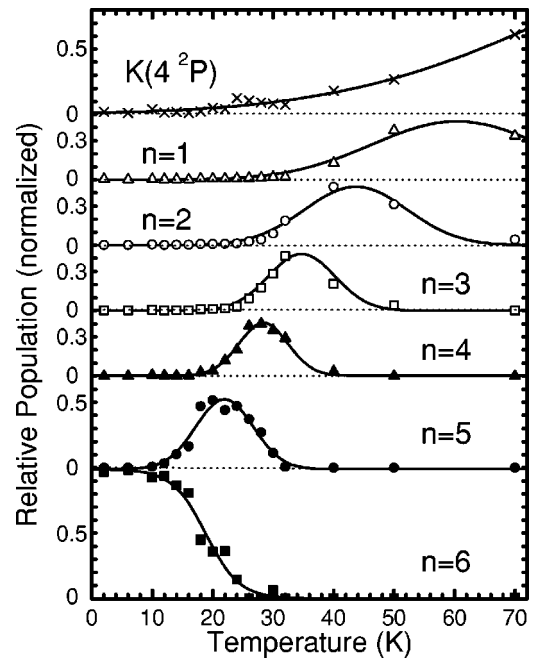

FIG. 3. Temperature dependence of the relative populations for K*He$_n$ ($n=1-6$) and $K(4\,{}^2P)$. Solid lines are guides for the eye.
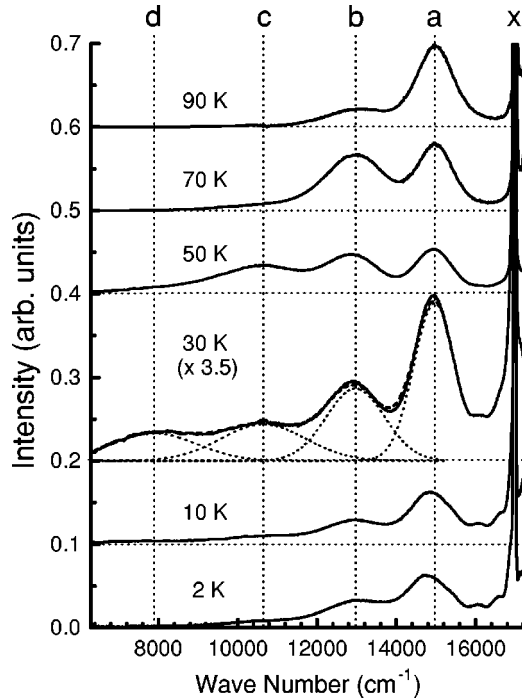
FIG. 4. Emission spectra of Na*He$_n$ in the case of D_2 excitation at various temperatures in gaseous He (solid lines). They are normalized by the total intensity integrated over $\nu > 6300$ cm^{-1}. The superposition curve (dashed line) of four Gaussian curves (dotted lines) is fitted to the spectrum observed at 30 K. Vertical dotted lines labeled as $a-d$ indicate the peak positions of the four Gaussian curves for $n = 1-4$, respectively. Sharp emission line labeled as x is the D emission line of atomic Na.
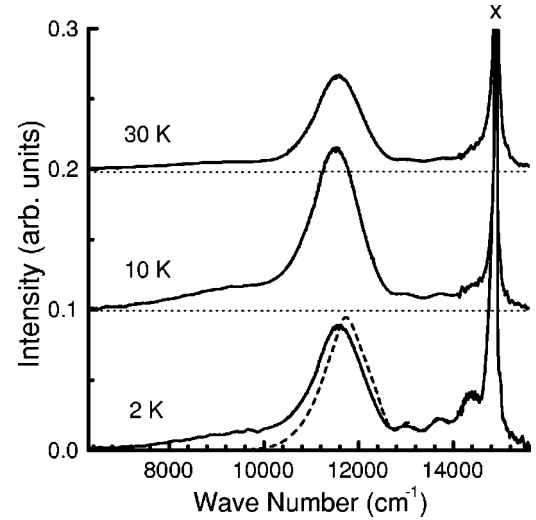

FIG. 5. Emission spectra of Li*He$_n$ at various temperatures in gaseous He (solid lines). The dashed line is the best-fitted superposition of theoretical emission spectra from different vibrational states of Li*He. Sharp emission line labeled as x is the D emission line of atomic Li.

$g_n(\nu)$ is the spectral profile for K*He$_n$. I is proportional to $N_n \int |\langle \psi_e | \psi_g(\nu) \rangle|^2 d\nu$, where $|\psi_e\rangle$ is the vibrational state of the electronic excited state and $|\psi_g(\nu)\rangle$ is the continuum state of the electronic ground state. Note that it is not necessary to calculate the Franck-Condon factor $|\langle \psi_e | \psi_g(\nu) \rangle|^2$, since $|\psi_g(\nu)\rangle$ forms a complete set and $\int |\langle \psi_e | \psi_g(\nu) \rangle|^2 d\nu = \langle \psi_e | \psi_e \rangle = 1$. Therefore, I is proportional to N_n. The temperature dependence indicates that the sticking He atoms gradually detached from exciplexes as the temperature was increased. Compared with the result for Rb*He$_n$, whose n_{max} is also six [13], the population transfer from $n = 6$ to $n = 0$ occurs at higher temperature under the same He gas density $(9 \times 10^{19}$ cm$^{-3})$. For example, the temperatures where the populations for $n = 5$ and $n = 1$ become maximum are about 18 K and 34 K for Rb*He$_n$, and are about 22 K and 60 K for K*He$_n$, respectively. This result indicates that the dissociation energies for the processes K*He$_n$ $\rightarrow$ K*He$_{n-1}$ + He $(n = 1-6)$ are about $1.2-1.8$ times larger than those for Rb*He$_n$ $\rightarrow$ Rb*He$_{n-1}$ + He. We also point out that at a low temperature around 2 K K*He$_n$ $(n > 2)$ are largely populated, while Rb*He$_n$ $(n > 2)$ are not. This difference can be attributed to the difference of the spin-orbit coupling strength. In the previous paper [13], we have shown that the spin-orbit coupling generates a potential barrier along the process of M*He$_2$ + He $\rightarrow M$*He$_3$, and this barrier is responsible for the fact that Rb*He$_n$ $(n > 2)$ are seldom

produced at about 2 K in gaseous He. Since the spin-orbit coupling is weaker for K, the effect of the barrier is considered to be smaller, which agrees with this experimental result. We will calculate the potential barrier for K in Sec. IV B.

Emission spectra of Na*He$_n$ in gaseous He at various temperatures are shown in Fig. 4. These emission spectra were measured with the PMT system in the range 6300–10 500 cm^{-1} and with the CCD system in the range $\nu > 10\,500$ cm^{-1}. In Fig. 4, we see clearly four broadband spectral components at about 15 000 cm^{-1}, 13 000 cm^{-1}, 10 600 cm^{-1}, and 7900 cm^{-1} in addition to the D lines. Since these peaks have almost the same interval, above four components are assigned to be emission spectra of Na*He$_n$ $(n = 1-4)$, respectively. In the wave-number range shown in Fig. 4, the ratio of the integrated fluorescence intensity from exciplexes to the total integrated intensity was about 0.5 at $T < 70$ K and it decreased with increase of temperature from 70 K. The fluorescence intensities for $n = 3$ and 4 became maximum around $30-50$ K. We fitted superposition of four Gaussian curves to all of the observed spectra shown in Fig. 4, similarly to the K case. The obtained peak positions and widths (FWHM) of spectral components are listed in Table I. Note that we have neglected the component for Na*He$_5$ which may overlap with the red tail of the component for Na*He$_4$. Therefore, the obtained wave number at the peak of the component for Na*He$_4$ may be smaller than the true value.

Emission spectra of Li*He$_n$ observed in gaseous He are shown in Fig. 5. The ratio of the integrated intensity of the emission from exciplexes to the total integrated intensity was about 0.5 at $T < 30$ K. There are several small spectral components in the range from the D line to about 12 000 cm^{-1} and a large component at about 11 600 cm^{-1}. These components are assigned to be from different vibrational states of Li*He. The largest spectral component at about

11 600 cm^{-1} is mainly from the vibrational ground state, and the other small components near the D line are from vibrational excited states. In Fig. 5, we also show an example of the best-fitted superposition (dashed line) of theoretical emission spectra from different vibrational states of Li*He. In calculation of emission spectra, we have used Pascale's theoretical adiabatic potential curves and transition moment [1], neglecting the fine structure since the splitting is quite small (0.3 cm^{-1} for atomic Li [21]). With this fitting, we found that the vibrational ground state was populated by about 70% of Li*He at 2 K. Compared to the best-fitted curve, the observed spectrum has a wide wing at the red side of the largest component, which cannot be accounted for as emission from Li*He. The peak position and the width (FWHM) of this weak component were roughly estimated to be $\sim$9000 cm^{-1} and $\sim$2000 cm^{-1}, respectively. The peak positions of this component, the component from the vibrational ground state of Li*He, and the D line are roughly equidistant. Therefore, we consider that the component at $\sim$9000 cm^{-1} is from Li*He$_2$. The peak position and width of the emission spectrum of Li*He were obtained by fitting single Gaussian curve to the largest component in Fig. 5, and the result is shown in Table I.

For light alkali-metal atoms such as K and Na, it is easy to distinguish the spectral component for each n, because the separation of components with different n is large compared to that of heavy alkali-metal atoms. Differently from the Rb case [13], this favorable feature allows us to assign easily the spectra of M*He$_n$ without any help of theoretical calculations.

IV. ANALYSIS WITH *AB INITIO* POTENTIAL CALCULATION

A. Confirmation of assignment

In the preceding section, we have assigned the observed spectra experimentally. To confirm the assignment, we carried out *ab initio* calculation of adiabatic potential curves. We used the MOLPRO program package [22]. We adopted 6-311G** basis sets [23,24] and performed the spin-restricted Hartree-Fock (RHF) calculation. The RHF calculation enables us to calculate vibrational energies easily. We calculated adiabatic potential curves of the lowest two electronic states, the excited $\widetilde{A}$ state and the ground $\widetilde{X}$ state, of M*He$_n$ for the symmetrical geometry. Namely, we fixed an alkali-metal atom at the center of a circle with a radius r, on which n He atoms were distributed equidistantly, and calculated potential energies as functions of r. Then we shifted the calculated potential curve so that the energy difference between the $\widetilde{A}$ and $\widetilde{X}$ states at $r=\infty$ coincides with the spin-orbit-averaged energy difference between the first P state and the ground S state of the alkali-metal atom M (13 023.6 cm^{-1} for K, 16 967.6 cm^{-1} for Na, and 14 903.9 cm^{-1} for Li [21]). Figure 6 shows the theoretical adiabatic potential curves for the $A\,^2\Pi$ and $X\,^2\Sigma$ states of K-He, Na-He, and Li-He obtained with the RHF calculation. The potential curve for the $A\,^2\Pi$ state is attractive, and the potential well becomes deeper for the lighter alkali-metal
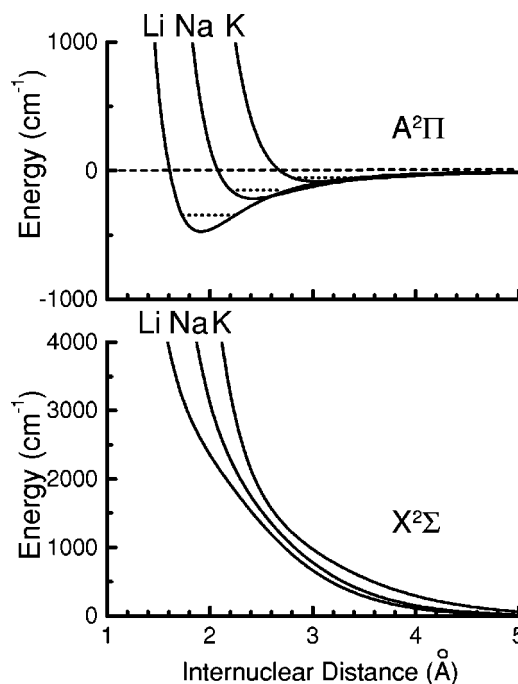

FIG. 6. Theoretical adiabatic potential curves for the $A\,^2\Pi$ and $X\,^2\Sigma$ states of K-He, Na-He, and Li-He obtained with the RHF calculation. The dotted lines show the energies of the rovibrational ground states. The spin-orbit coupling is not included. The zero energy corresponds to the energy at the dissociation limit.

atom. The potential curve for the $X\,^2\Sigma$ state is almost repulsive. In the present calculation we did not take into account the fine-structure splitting of the exciplexes, since the fine-structure splitting of light alkali-metal atoms in the first P state is negligibly small (57.7 cm^{-1} for K, 17.2 cm^{-1} for Na, and 0.3 cm^{-1} for Li [21]). The strength of the spin-orbit coupling in M*He$_n$ exciplexes is considered to be almost the same as that in the alkali-metal atoms in the first P state, similarly to other van der Waals complexes of an alkali-metal-like atom and an Ar atom [25].

We also calculated the sum ϵ_v of zero-point energies of all vibrational modes in the $\widetilde{A}$ state [26,27]. At the equilibrium radius r_e for the $\widetilde{A}$ state, we will write the potential energies of the $\widetilde{A}$ and $\widetilde{X}$ states relative to the dissociation limit of the $\widetilde{X}$ state as ϵ_A and ϵ_X, respectively. Figure 7 shows the calculated values of ϵ_A, ϵ_X, ϵ_v, and r_e for K*He$_n$, Na*He$_n$, and Li*He$_n$. The energies of the rovibrational ground states, given by $\epsilon_A+\epsilon_v$, are shown by dashed lines. The peak position of the emission spectrum of M*He$_n$ is roughly approximated by the difference ν_P between the energy of the rovibrational ground state in the $\widetilde{A}$ state and the potential energy in the $\widetilde{X}$ state at $r=r_e$, that is, $\nu_P=\epsilon_A+\epsilon_v-\epsilon_X$. The values of ν_P for K*He$_n$, Na*He$_n$, and Li*He$_n$ are listed in Table II. Comparing these theoretical values to the experimental ones listed in Table I, the deviation between them per He atom is less than 162 cm^{-1} for K*He$_n$ and 373 cm^{-1} for Na*He$_n$. In the case of Li*He$_n$, the deviation is 417 cm^{-1} for Li*He, and about 1400 cm^{-1} for Li*He$_2$. Except for Li*He$_2$, we can say that the theoretical peak positions
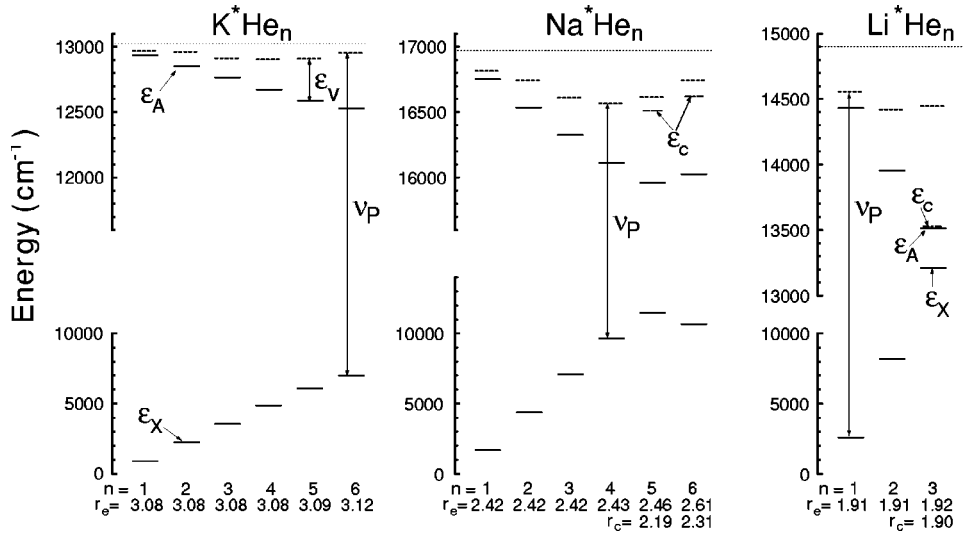
FIG. 7. Theoretical values of ϵ_A (solid lines), ϵ_X (solid lines), and $\epsilon_A + \epsilon_v$ (dashed lines) of each exciplex $M^*\text{He}_n$. The equilibrium radius r_e (in Å) is also shown. The dotted lines indicate the spin-orbit-averaged energy levels of the first excited P state of alkali-metal atoms relative to the level of the ground S state. The energy ϵ_c (dash-dotted lines) and the radius r_c (in Å) at the level crossing point are shown for Na*He$_n$ ($n=5,6$) and Li*He$_3$. The energy differences labeled as ν_P indicate approximate values of peak positions of emission spectra of the exciplexes.

roughly coincide with the experimental ones, so that the assignments given in Sec. III are confirmed. The reason for the large deviation for Li*He$_2$ has not been found yet.

Among potential curves for the $A\,^2\Pi$ state of M^*He, only the potential curve for Li*He has been precisely evaluated so far by Havey and co-workers with the spectroscopic study on the $3d\,^2\Delta \leftarrow 2p\,^2\Pi$ bound-bound transition [8,9]. They have reported that the potential-well depth is 1020(20) cm^{-1}, which is much larger than our RHF calculation (473.3 cm^{-1}). Such inaccuracy of the RHF calculation results in disagreement between theoretical and experimental values of n_{max}. Theoretical calculation shows that K*He$_4$, Na*He$_4$, and Li*He$_2$ have the lowest energies, and hence they are expected to be the terminal exciplexes. This theoretical result, however, disagrees with our experimental result that $n_{\text{max}}=6$ for K. Similarly, we cannot conclude that Na*He$_4$ and Li*He$_2$ are the terminal exciplexes. Even if Na*He$_n$ ($n>4$) and Li*He$_n$ ($n>2$) are formed, we cannot detect their fluorescence in the present study, because the wave numbers of their spectra are expected to be out of the range of our detectors. For example, the emission spectrum of Na*He$_5$ is estimated to be seen around 5000 cm^{-1} by extrapolating the peak position interval obtained experimentally. Furthermore, for Na*He$_n$ ($n=5,6$) and Li*He$_3$, the calculated potential curves of the $\widetilde{A}$ and $\widetilde{X}$ states as functions of radius r show the crossing below the energy of the rovibrational ground state. Because of this level crossing, it is possible that the fluorescence from Na*He$_n$ ($n=5,6$) and

Li*He$_3$ is quenched. The radius r_c and the energy ϵ_c at the crossing point are also shown in Fig. 7. We see that ϵ_c for Li*He$_3$ is largely below the rovibrational ground level, so that it is quite probable for Li*He$_3$ that the quenching of the fluorescence occurs.

B. Calculation of potential barrier

As mentioned in Sec. III, the emission from K*He$_6$ is much stronger than that from Rb*He$_6$ at $T=2$ K. To explain this, we calculated the potential barrier for the process of K*He$_2$ + He $\rightarrow$ K*He$_3$. The procedure of the calculation was similar to that in Ref. [13]. We fixed the geometry of K*He$_2$ to the equilibrium one: a K atom was located at $(x,y) = (0,0)$ and two He atoms were at $(0,\pm 3.08)$ (in units of Å). Locating the third He atom at various points in the xy plane, we calculated the adiabatic potential surfaces for the lowest three electronic excited states, all of which are correlated with the first P state of the K atom. The wave functions of the valence electron in these electronic states are well expressed by p_ξ, p_η, p_z orbitals, where ξ and η axes are chosen so that the interaction Hamiltonian without the spin-orbit coupling becomes diagonal for the bases of p_ξ, p_η, p_z orbitals. Therefore, under the assumption that the strength of the spin-orbit coupling is not changed by the approach of He atoms, the interaction Hamiltonian including the spin-orbit coupling can be written in terms of the bases $[p_\xi, p_\eta, p_z]$ as

$$\begin{pmatrix} E_\xi & -i\Delta_{so}/3 & \Delta_{so}/3 \\ i\Delta_{so}/3 & E_\eta & -i\Delta_{so}/3 \\ \Delta_{so}/3 & i\Delta_{so}/3 & E_z \end{pmatrix}, \qquad (1)$$

where Δ_{so} is the fine-structure splitting energy of K in the $4\,^2P$ state (57.7 cm^{-1}), and E_ξ, E_η, E_z are the potential energies corresponding to the p_ξ, p_η, p_z orbitals, respectively. Diagonalizing the matrix (1) for each location of the third He atom, we obtained one attractive and two repulsive potential surfaces. The attractive potential surface is shown as a contour map for the location of the third He atom in Fig. 8. The potential minimum is located at $(x,y) = (3.1,0)$, and the

TABLE II. Theoretical peak position (ν_P in cm^{-1}) of the emission spectrum of each exciplex $M^*\text{He}_n$.

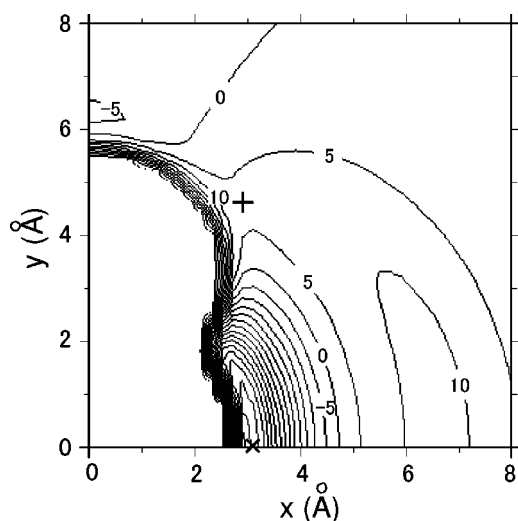| n	K*He$_n$	Na*He$_n$	Li*He$_n$
1	12 076	15 113	11 970
2	10 707	12 357	6213
3	9365	9530	1237
4	8025	6902	
5	6781	5107	
6	5943	6079	

FIG. 8. Potential-energy surface calculated for the system of K^*He_2-He including the spin-orbit coupling. The K atom is fixed at $(x,y)=(0,0)$ and the two He atoms of K^*He_2 are fixed at $(0, \pm 3.08)$ in unit of Å. The energy in unit of cm^{-1} is measured from the dissociation limit $K^*He_2(\tilde{A}\,^2\Pi_{1/2})+$He. The contour interval is $5\ cm^{-1}$. The marks "+" and "×" indicate the positions of the saddle point and the potential minimum, respectively.

depth is $69\ cm^{-1}$ from the dissociation limit K^*He_2 $(\tilde{A}\,^2\Pi_{1/2})+$He. There is a saddle point at $(2.9,4.6)$, and the height is $5.8\ cm^{-1}$ which is about 1/4 of that in the Rb case $(20.5\ cm^{-1})$. In the case of Rb, the effect of the potential barrier becomes negligible at $T\sim 10$ K [13]. Therefore, in the case of K, it is plausible to consider that the effect of the potential barrier is also negligible at $T\sim 2$ K.

V. CONCLUSION

We have reported emission spectra of K^*He_n ($n=1$ -6), Na^*He_n ($n=1-4$), and Li^*He_n ($n=1,2$) in the spec-

tral range $\nu > 6300\ cm^{-1}$, by exciting alkali-metal atoms produced in cold gaseous He with the laser ablation method. To our knowledge, this is the first observation of the emission spectra of K^*He_n ($n\geqslant 3$), Na^*He_n ($n\geqslant 3$), and Li^*He_2. We also observed the fluorescence from $K^*He_{n_{max}}$ in liquid He, and the value of n_{max} was found to be six. We obtained the peak position and the width of the spectral component of each M^*He_n. The assignment was made experimentally, since the emission spectra of M^*He_n with different n are well separated. We confirmed the assignment of the observed spectra by performing *ab initio* calculation at the RHF level. The theoretical peak positions roughly agree with experimental ones, except for Li^*He_2. We also calculated the potential surface for the system of K^*He_2+He, to estimate the potential barrier generated by the spin-orbit coupling.

Now, the emission spectra of all alkali-metal$-$He exciplexes from Cs^*He_n to Li^*He_n in the near infrared region have been observed. These extensive studies will help the improvement of accuracy of theoretical calculations. The investigation on Na^*He_n ($n>4$) and Li^*He_n ($n>2$) is remained as future work, and it may reveal whether the quenching process really occurs or not.

[1] J. Pascale, Phys. Rev. A **28**, 632 (1983).

[2] R.E.M. Hedges, D.L. Drummond, and A. Gallagher, Phys. Rev. A **6**, 1519 (1972).

[3] D.L. Drummond and A. Gallagher, J. Chem. Phys. **60**, 3426 (1974).

[4] G. York, A.R. Scheps, and A. Gallagher, J. Chem. Phys. **63**, 1052 (1975).

[5] R. Scheps, Ch. Ottinger, G. York, and A. Gallagher, J. Chem. Phys. **63**, 2581 (1975).

[6] M.D. Havey, S.E. Frolking, and J.J. Wright, Phys. Rev. Lett. **45**, 1783 (1980).

[7] L.C. Balling, J.J. Wright, and M.D. Havey, Phys. Rev. A **26**, 1426 (1982).

[8] M.D. Havey, Phys. Rev. Lett. **48**, 1100 (1982).

[9] C.J. Lee, M.D. Havey, and R.P. Meyer, Phys. Rev. A **43**, 77 (1991).

[10] J. Dupont-Roc, Z. Phys. B: Condens. Matter **98**, 383 (1995).

[11] S. Kanorsky, A. Weis, M. Arndt, R. Dziewior, and T.W. Hän-

sch, Z. Phys. B: Condens. Matter **98**, 371 (1995).

[12] K. Enomoto, K. Hirano, M. Kumakura, Y. Takahashi, and T. Yabuzaki, Phys. Rev. A **66**, 042505 (2002).

[13] K. Hirano, K. Enomoto, M. Kumakura, Y. Takahashi, and T. Yabuzaki, Phys. Rev. A **68**, 012722 (2003).

[14] G. DeToffol, F. Ancilotto, and F. Toigo, J. Low Temp. Phys. **102**, 381 (1996).

[15] F. Stienkemeier, J. Higgins, C. Callegari, S.I. Kanorsky, W.E. Ernst, and G. Scoles, Z. Phys. D: At., Mol. Clusters **38**, 253 (1996).

[16] J. Reho, C. Callegari, J. Higgins, W.E. Ernst, K.K. Lehmann, and G. Scoles, Faraday Discuss. **108**, 161 (1997); J. Reho, J. Higgins, C. Callegari, K.K. Lehmann, and G. Scoles, J. Chem. Phys. **113**, 9686 (2000).

[17] J. Reho, J. Higgins, K.K. Lehmann, and G. Scoles, J. Chem. Phys. **113**, 9694 (2000).

[18] F.R. Brühl, R.A. Trasca, and W.E. Ernst, J. Chem. Phys. **115**, 10220 (2001).

[19] C.P. Schulz, P. Claas, and F. Stienkemeier, Phys. Rev. Lett. **87**, 153401 (2001).

[20] Z.J. Jakubek, Q. Hui, and M. Takami, Phys. Rev. Lett. **79**, 629 (1997).

[21] A. A. Radzig and B. M. Smirnov, *Reference Data on Atoms, Molecules, and Ions* (Springer-Verlag, New York, 1985).

[22] R. D. Amos, A. Bernhardsson, A. Berning, P. Celani, D. L. Cooper, M. J. O. Deegan, A. J. Dobbyn, F. Eckert, C. Hampel, G. Hetzer, P. J. Knowles, T. Korona, R. Lindh, A. W. Lloyd, S. J. McNicholas, F. R. Manby, W. Meyer, M. E. Mura, A. Nicklass, P. Palmieri, R. Pitzer, G. Rauhut, M. Schütz, U. Schumann, H. Stoll, A. J. Stone, R. Tarroni, T. Thorsteinsson, and H.-J. Werner, MOLPRO, version 2002.1, a package of *ab initio* programs designed by H.-J. Werner and P. J. Knowles.

[23] R. Krishnan, J.S. Binkley, R. Seeger, and J.A. Pople, J. Chem. Phys. **72**, 650 (1980).

[24] J-P. Blaudeau, M.P. McGrath, L.A. Curtiss, and L. Radom, J. Chem. Phys. **107**, 5016 (1997).

[25] See, for example, J.S. Pilgrim, C.S. Yeh, K.R. Berry, and M.A. Duncan, J. Chem. Phys. **100**, 7945 (1994); L.R. Brock and M.A. Duncan, J. Chem. Phys. **103**, 9200 (1995).

[26] R. Lindh, Theor. Chim. Acta **85**, 423 (1993).

[27] G. Rauhut, A. El Azhary, F. Eckert, U. Schumann, and H.-J. Werner, Spectrochim. Acta, Part A **55**, 647 (1999).